Inorganica Chimica Acta 363 (2010) 3847–3855

Contents lists available at ScienceDirect

Inorganica Chimica Acta

journal homepage: www.elsevier.com/locate/ica

# Spectroscopic speciation and structural characterisation of uranyl(VI) interaction with pyridine carboxylic acid N-oxide derivatives

Stefan Lis [a,*], Guenther Meinrath [b], Zbigniew Glatty [a], Maciej Kubicki [a]

[a] Faculty of Chemistry, Adam Mickiewicz University, Grunwaldzka 6, 60-780 Poznań, Poland
[b] RER Consultants, Schiessstattweg 3a, D-94032 Passau, Germany

ARTICLE INFO

*Article history:*
Received 11 November 2009
Received in revised form 7 July 2010
Accepted 12 July 2010
Available online 22 July 2010

*Keywords:*
Uranyl(VI)
Pyridine carboxylic acid N-oxides
Spectroscopic speciation
Single component spectra
Thermodynamic data
Crystal structure

ABSTRACT

Spectroscopic speciation of U(VI) solutions holding pyridine carboxylic acid N-oxides in a range pH 2.3–4.5 results in the single component spectrum of the U(VI) isonicotinic acid N-oxide complex. The molar absorption is 14 ± 2 L mol$^{-1}$ cm$^{-1}$ at 415.4 nm. The formation constant lg $K_{UL}$ = 2.1 ± 0.2 ($k$ = 2) is derived from solution modelling and by multivariate chemometric analysis. The first crystal structure analysis of a U(VI) pyridine carboxylic acid N-oxide revealed a sheet-like structure where the isonicotinic acid N-oxide binds to the uranyl(VI) both bidentately by the carboxylate group and monodentately by the N–O group. The single component spectrum of the $[UO_2L]^+$ (where $L^-$ is isonicotinate N-oxide) is compared to the small number of other U(VI) single ligand species. The comparison revealed the possible pitfalls of U(VI) spectroscopic speciation close to the pH region where U(VI) hydrolysis starts to interfere. On basis of the results for U(VI)–L coordination and physicochemical properties of the pyridine carboxylic acid N-oxides some conclusions could be drawn on the likely behaviour of nicotinic acid N-oxide and picolinic acid N-oxide. For the former, complex formation in a narrow range of pH and U(VI) concentrations close to the hydrolysis range of U(VI) might reveal thermodynamic data. In the case of picolinic acid N-oxide, additional experimental evidence is required to characterize suitable conditions.



## 1. Introduction

This study aims on the characterisation of pyridine carboxylic acid N-oxides interaction with hexavalent uranium. The respective compounds are picolinic acid N-oxide (picNO), nicotinic acid N-oxide (nicNO) and isonicotinic acid N-oxide (isonicNO). In the following discussion, focus is given to spectroscopic speciation of isonicotinic acid N-oxide (isonicNO). Isonicotinic acid N-oxide (HL) is a weak acid whose acidity constant p$K_{HL}$ is close to the onset of U(VI) hydrolysis. Thus, quantitative spectroscopic speciation is required to avoid misinterpretation of the observations due to interference by hydrolysis. In addition, the low solubility of HL in acidic aqueous solution limits the concentration range available for investigation. Despite the narrow boundaries set by the system of interest evidence will be forwarded that single component spectra of relevant species are unambiguously obtained by applying the spectra to the resolution of multi-component spectra.

Pyridine N-oxides have applications in wide range of fields including, for instance, industry, medicine, biochemistry and nanotechnology [1–8]. They are, for instance, studied for their use as versatile synthetic intermediates [1–3] and investigated as a new class of antiviral compounds [3]. The surprisingly small database on the solution behaviour of these compounds has triggered a series of studies focusing on interaction with fluorescent lanthanides in aqueous and non-aqueous solutions [5–7]. Structural and spectroscopic information has recently been reported for compounds with transition metals and lanthanides [5–8]. Uranyl(VI) is a fluorescent center where fluorescence is influenced by coordinating ligands in various ways. Spectroscopic speciation of fluorescent metal ions allows characterisation of metal ligand interactions by multiple parameters, e.g. absorption, excitation and time-resolved fluorescence spectroscopy [9–12]. Hexavalent uranium occurs almost exclusively as uranyl $UO_2^{2+}$. The $UO_2^{2+}$ entity is always linear with O–U–O bond angles close to 180°. The uranyl group is coordinated in the equatorial plane by 4, 5, or 6 ligands. Bond lengths to the equatorial ligands are always larger than to the axial uranyl oxygens. While uranyl(VI) is a suitable fluorescent center, complex formation with pyridine carboxylic acids N-oxides has not been reported before the advent of this study. Information on the related U(VI) pyridine carboxylic acids is similarly scarce [13–15].

The study of uranyl solution behaviour and related spectroscopic properties until recently has been hampered by contradictory observations and concepts [10,16–20]. A predominant reason has been the hydrolytic behaviour of U(VI) forming distinct oligomeric species $(UO_2)_2(OH)_2^{2+}$ and $(UO_2)_3(OH)_5^+$ [21]. The characteristic UV–Vis absorption band at 413 nm for $UO_2^{2+}$(aq) has a very low molar absorption of 9.7 L mol$^{-1}$ cm$^{-1}$ [10,17] while the

* Corresponding author. Tel.: +48 61 829 1345; fax: +48 61 829 1505.
*E-mail address:* blis@amu.edu.pl (S. Lis).

0020-1693/$ - see front matter © 2010 Elsevier B.V. All rights reserved.
doi:10.1016/j.ica.2010.07.025

oligomeric hydrolysis species have molar absorptions of 101 L mol$^{-1}$ cm$^{-1}$ at 421.8 nm and 474 L mol$^{-1}$ cm$^{-1}$ at 429 nm, respectively [22]. In addition, various additional species have been inferred from early curve-fitting exercises ignoring statistical significance. For species like $(UO_2)_4(OH)_7^+$ or $(UO_2)_2(OH)^+$ [23], single component spectra for UV–Vis absorption and emission have never been reported while for $(UO_2)_2(OH)_2^{2+}$ and $(UO_2)_3(OH)_5^+$ single component spectra and their successful application in spectroscopic speciation of various systems are demonstrated [10,22,24–26]. Due to the significant influence U(VI) hydrolysis contributes to studies of solution chemistry behaviour even at slightly acidic media, most published information especially on the single ligand species requires clarification [19,20].

Symmetry plays an important role in the interpretation of uranyl(VI)) spectra [27,28]. Evidence has been put forward illustrating a correlation of the U(VI) UV–Vis absorption and vibronic spectra with the symmetry of equatorial coordination [27–29]. This correlation has been helpful in interpreting single component absorption spectra of U(VI) carbonato species with two and three carbonate ligands [30]. For the single ligand species, however, evidence is less clear as will be outlined on basis of the results from this study.

Thus, this investigation has been motivated by four reasons: improving the rather poor database on pyridine carboxylic acid N-oxide behaviour in aqueous solutions, analysis of a complex and susceptible chemical interaction in aqueous solution by chemometric methods, extending the database of single component spectra for defined U(VI) species and to correlate the results with existing hypotheses on the correlation of U(VI) UV–Vis absorption spectra with coordination symmetry. From the results obtained on the four reasons, a more profound insight into U(VI) interaction with pyridine carboxylic acid N-oxides was intended in order to find suitable conditions for analogous studies of nicNO and picNO. For these both isomers solution behaviour is still unknown. From the thermodynamic results of this study on U(VI) isonicNO complexation, conclusions on the stability of U(VI) nicNO complexation will be drawn.

## 2. Experimental

### 2.1. Apparatus and data collection

A CP-415 pH-meter with OSH 10–10 combined glass pH electrode was used for all pH measurements. Calibration of the pH-meter was performed using 5-point calibration as recommended by IUPAC. Merck Co. (Germany) buffer standards have been used. A Shimadzu UVPC 2401 spectrophotometer with 1 cm quartz cuvettes was used to record spectra in the wavelength range 400–800 nm.

In total 80 spectra have been recorded in the range pH 2–5. Concentrations in the range $10^{-5}$ mol dm$^{-3}$ < [U(VI)] < $5 \times 10^{-2}$ mol dm$^{-3}$ and $10^{-4}$ mol dm$^{-3}$ < [HL] < $2 \times 10^{-2}$ mol dm$^{-3}$. From this data set, nine spectra indicated U(VI)-HL interaction. The majority of spectra was either contaminated by hydrolysis or unaffected by coordination.

### 2.2. Reagents

Uranyl nitrate stock solution was prepared from uranyl acetate dehydrate salt (P.O.Ch. Gliwice, Polish Company), which was previously placed into a muffle oven at 1073 K for 2 h. Obtained uranyl oxide $U_3O_8$ was then dissolved in 6 M HCl with addition of solid Zn to get rid of $UO_2Cl_2$ and heated with stirring. To the greenish solution of $UCl_4$ water was added and by gently heating evaporated to remove HCl. Picolinic acid N-oxide, nicotinic acid N-oxide, and isonicotinic acid N-oxide were obtained from commercially available reagents (Aldrich) without further purification. Acetonitrile ($CH_3CN$), dimethyl sulphoxide (DMSO) and dimethyl formamide (DMF) were obtained from commercially available sample (Aldrich), methanol and 1,4-dioxane were obtained from P.O.Ch. Gliwice/PL.

### 2.3. Synthesis of single crystals

The uranium tetrachloride solution was diluted (up to 0.05 M) and its concentration has been checked spectroscopically (solution A). 0.7 g (5 mmol) of isonicotinic acid N-oxide was added to 90 ml of water in 200 ml baker. The mixture was heated (80 °C) for 5 min. and stirred on the stirring bar. After cooling down it was transferred to the volume flask (100 ml) and filled up using water to obtain the total concentration 0.05 M (solution B). To solution A (25 ml) solution B (25 ml) was added slowly dropwise with stirring.

The mixture was gently heated in the beaker for 1 h, cooled down and then let to crystallize in room temperature. The resultant solution was filtered off. Storage of the solution in a desiccator for several days yielded crystals of the complex $[UO_2Cl(HisonicNO)(isonicNO)]_n$. The analysis was made with a KUMA KM4CCD four-circle diffractometer equipped with a CCD (Charge Coupled Device) detector.

The carbon, hydrogen and nitrogen content of the compound were determined by elemental analysis on an Elemental analyser model VARIO ELIII. The elemental analysis of the $UO_2Cl(HisonicNO)(isonicNO)$ compound showed the following data: C = 24.38%; H = 1.54%; N = 4.78%, which are in a very good agreement with the calculated values: C = 24.73%; H = 1.56%; N = 4.81% for $C_{12}H_9N_2O_8UCl$.

### 2.4. Data analysis

Spectral data was baseline corrected and analysed by multivariate analysis using the TBCAT (Threshold Bootstrap Target Factor Analysis) code. The code identifies single components from multi-component UV–Vis spectroscopic data on basis of factor analysis and Simplex optimisation using non-negativity of absorptions and species concentrations as well as known single components as optimisation criteria. Details are given in the text and related references. The major factors influencing the results, e.g. measurement uncertainty in the chemical amounts of metal ion and ligand, and numerical effects, e.g. non-linearity and non-normality, are taken into account. The numerical results are expressed as complete measurement uncertainties. The validity of results is further corroborated by numerical interpretation of multi-component spectra due to the identified single components. The TBCAT code is available in literature together with tutorial information and example spectra [31]. Further details are given in the text and related references.

## 3. Results and discussion

The structure of the three pyridine carboxylate N-oxides: isonicNO (I), nicNO (II) and picNO (III) are given schematically in Fig. 1. Table 1 summarises a few properties of interest: dipole moments, charge densities and acidity constants of the conjugate acids.

Table 1 shows that the acidity constant of picolinic acid N-oxide is within the pH region where U(VI) hydrolysis predominates, while for nicotinic acid N-oxide and isonicotinic acid N-oxide a small margin remains where an amount of dissociated ligand is available that might be sufficient to observe U(VI) ligand interaction [32–34]. This study focuses on isonicotinic acid N-oxide.

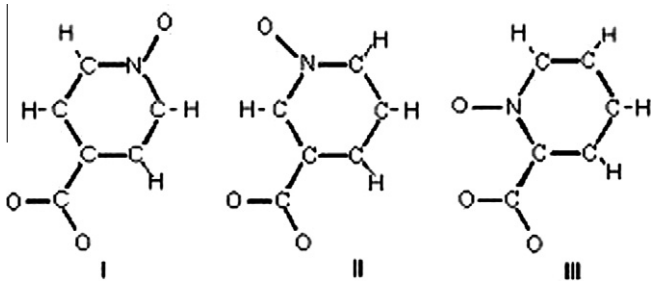

**Fig. 1.** Structural representations of isonicotinicate N-oxide (I), nicotinicate N-oxide (II) and picolinate N-oxide (III).

**Table 1**
Dipole moments and charge densities of pyridine carboxylic acid N-oxides.

| Ligand | Dipole moment ($D$)[a] | Charge densities[b] | Acidity ($pK_s$) |
|---|---|---|---|
| isonicNO | 9.0 | −0.980 | 2.9 [32] |
| nicNO | 14.8 | −0.844 | 2.63 ± 0.08 [33] |
| picNO | 16.3 | −1.047 (−1.473) | 3.63 ± 0.06 [33] |

[a] Calculated from GAUSSIAN 98 [34] at the B3LYP level using a PCM solvent model for water.

[b] Calculated from the SCF densities using the ChelpG approach; the figure in brackets gives the sum of charge densities for the carboxyl group and the neighboring N-oxide group.

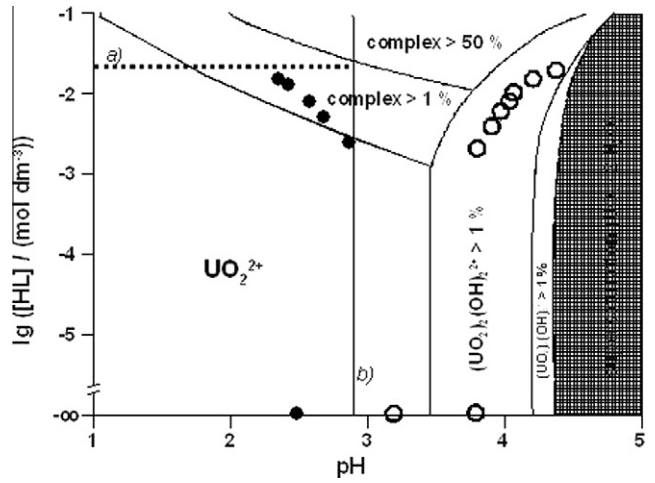


**Fig. 2.** Constraints in the system U(VI)/isonicotinic acid N-oxide. The dashed line (a) gives the solubility limit of HL. The vertical solid line (b) indicates the condition pH = $pK_{HL}$. The hashed field indicates precipitation of schoepite ($UO_3$ $2H_2O$) [39]. The stability fields of U(VI) species are obtained for a U(VI) total concentration of $2 \times 10^{-3}$ mol dm$^{-3}$ and derived from geochemical modelling as outlined in the text.

The system uranyl(VI)-isonicotinate N-oxide (U(VI)–L) is limited by four constraints: (a) the limited solubility of isonicotinic acid N oxide (HL) in aqueous solution, (b) the low molar absorption of $UO_2^{2+}$ in the characteristic absorption band at 413.8 nm, (c) the onset of U(VI) hydrolysis at values between pH 3.3 and 3.7 (depending on U(VI) total concentration) while lanthanides hydrolyse at values of about pH 5 and (d) the $pK_{HL}$ of isonicotinic acid N oxide close to U(VI) hydrolysis onset. Hence, complex formation can be studied in a very narrow range of experimental conditions – if there is any interaction at all.

Fig. 2 illustrates these constraints. The dashed line a gives the solubility of HL (HL: isonicotinic acid N-oxide). The solubility of HL in aqueous solution is $2 \times 10^{-2}$ mol dm$^{-3}$ [32]. The undissociated molecule does obviously not coordinate to U(VI). The concentration of $L^-$ increases with pH especially at values of pH close and above the value of $pK_{HL}$. The value of $pK_{HL}$ is indicated by the vertical line b in Fig. 2. UV–Vis spectroscopy is a feasible method to identify the specific state of U(VI) in aqueous solutions [9,25]. Due to the low molar absorption of the characteristic absorption band of U(VI) in the range 330–550 nm the species $UO_2^{2+}$ can be spectroscopically identified only at rather high molar concentrations. The molar absorption of U(VI) rises with coordination [17,27,30]. In order to identify $UO_2^{2+}$ among other species by spectroscopic speciation, the minimum U(VI) amount should not be below $10^{-5}$ mol dm$^{-3}$. Hydrolysis products of U(VI) above this U(VI) concentration threshold are oligomeric: [21] $(UO_2)_2(OH)_2^{2+}$ and $(UO_2)_3(OH)_5^+$. These species form close to the solubility limit of U(VI). Fig. 2 gives stability fields of the both hydrolysis products where the respective relative concentration is above 1%. Due to the high molar absorption of these species they nevertheless will dominate the observed absorption spectra. Thus identification of other species will become rather difficult even if that other species might have the higher relative concentration.

There are further oligomeric hydrolysis products reported in literature, e.g. $(UO_2)_4(OH)_7^+$ [10,18,23,35]. However, during the extensive spectroscopic studies in the past almost two decades, we have been unable to identify even a single of these additional oligomeric species. Repeated studies of saturated and unsaturated U(VI) solutions using UV–Vis spectroscopy [26] and laser-induced time-resolved fluorescence spectroscopy [36,37] indicated that all hydrolysed solutions could be numerically interpreted by the single component spectra of $(UO_2)_2(OH)_2^{2+}$ and $(UO_2)_3(OH)_5^+$. This finding is further corroborated in this study and examples will be given. Due to the oligonuclear nature of these species the stability fields depend on the total U(VI) concentration. The lower the total U(VI) concentration the higher the pH at which hydrolysis starts. Fig. 2 is derived for a U(VI) total concentration of $10^{-2}$ mol dm$^{-3}$. Spectroscopic speciation has also performed at lower U(VI) total concentrations, but the discussion will be based on the data obtained at U(VI) concentration of 0.01 mol dm$^{-3}$. The spectra obtained at lower U(VI) concentrations have been included in the quantitative data evaluation by chemometric methods.

The interest focused on the question to what extent complex formation with the ligand L can be observed and quantitatively interpreted in terms of single component spectra and formation constants of the U(VI)–L species. Its formation constant will be given as

$$\log K_{UL} = \lg[UL^+] - \lg[L^-] - \lg[UO_2^{2+}] \quad (1)$$

where square brackets indicate molar concentrations.

Due to the narrow margin left by the constraints, a formation constant can be estimated already on basis of solution conditions indicating onset of complex formation. This value subsequently may be compared to the result of numerical evaluations using spectroscopic speciation in combination with chemometric evaluation tools on basis of multivariate analysis [38]. Thus, two independent methods are available to estimate formation constants. The results for multivariate analysis, single component spectra of the solution species and molar absorptions, have been corroborated by their application in the deconvolution of UV–Vis spectra holding other species, e.g. hydrolysis products of U(VI).

The systematic screening of the U(VI)/HL system at various U(VI) total concentrations mainly indicated either $UO_2^{2+}$ solutions or hydrolysis. Fig. 3 gives a characteristic set of spectra collected for conditions under hydrolysis in the region pH 3.20–4.54. At a given total U(VI) concentration of $1 \times 10^{-2}$ mol dm$^{-3}$, the maximum absorption rises from about 0.1 to about 0.7 cm$^{-1}$. This is due to the effect of hydrolysis, where the species $(UO_2)_2(OH)_2^{2+}$ $(UO_2)_3(OH)_5^+$ prevail. Fig. 4 shows a deconvolution of the spectrum

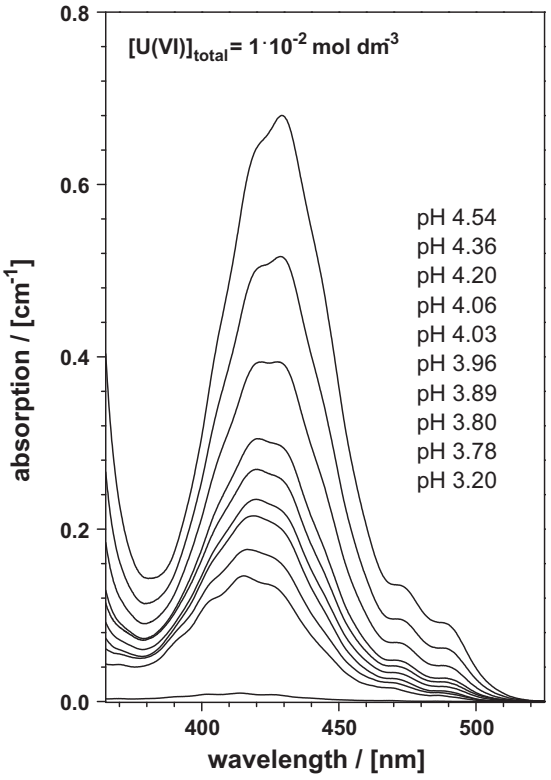


**Fig. 3.** UV–Vis absorption spectra obtained in the range pH 3.20–4.54 at a total U(VI) concentration of $2 \times 10^{-3}$ mol dm$^{-3}$. The spectra are related to the open circles in Fig. 2. The sequence of spectra from top to bottom relates to the sequence of value of pH at the right-hand-side.

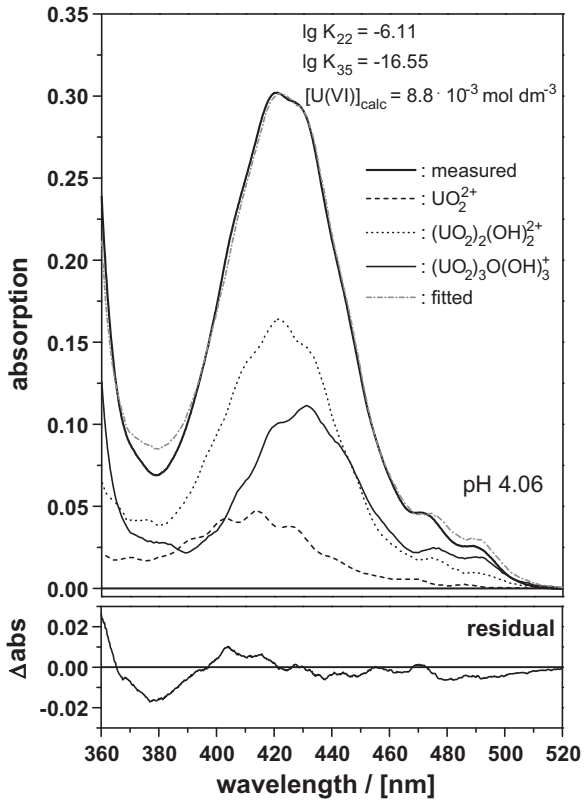


**Fig. 4.** Numerical interpretation (least squares fit) of an experimental spectrum at pH 4.06 by the single components $UO_2^{2+}$, $(UO_2)_2(OH)_2^{2+}$ and $(UO_2)_3(OH)_5^{+}$.

at pH 4.06. Despite the fact that the single component spectra of $(UO_2)_2(OH)_2^{2+}$ and $(UO_2)_3(OH)_5^{+}$ have been obtained in previous studies using different equipment at a different laboratory, they are able to interpret the observed spectrum at pH 4.06 satisfactorily. The parameters of the spectra shown in Fig. 3 are indicated in Fig. 2 by open circles. Thus, at pH 3.20, the spectrum of the hydrated $UO_2^{2+}$ is observed. At pH 3.78, hydrolysis occurs which proceeds with increasing pH. The solutions also hold HL and $L^-$ in increasing concentrations but no influence is observed. Obviously, the $L^-$ ligand appears to be too weak to compete with hydrolysis.

Among the spectra systematically collected, however, a set in the region pH 2–3 indicated a weak but systematic change in the characteristic UV–Vis absorption band of U(VI). This set is given in Fig. 5. From a heuristic assumption using the expertise collected during the past 20 years of research in uranium solution chemistry, the relative amount of the new species was estimated to be below 50%.

On basis of this judgment, the solution composition was modelled using the formation constants given in Table 2 [22,39]. From this modelling effort, the boundaries for various relative species concentrations given in Fig. 2 have been obtained. The observations are in agreement with a formation constant of the $UO_2L^+$ species, lg $K_{UL} = 2.1$.

Following this 'expert judgment', a strictly numerical interpretation was attempted applying multivariate analysis. For this purpose threshold bootstrap computer-assisted target factor analysis (TBCAT) was applied [38]. TBCAT is able to forward possible deconvolutions of multi-species spectra if at least one component of the

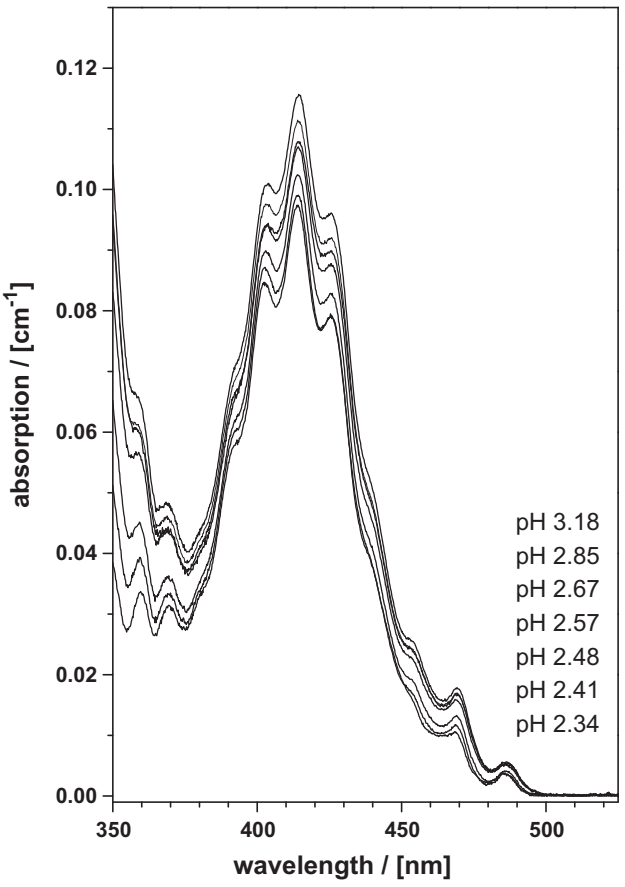


**Fig. 5.** UV–Vis absorption spectra recorded in the range pH 2.34–3.18 at total U(VI) concentration of $2 \times 10^{-3}$ mol dm$^{-3}$. The spectra relate to the solid circles in Fig. 2. The sequence of spectra in the absorption maximum follows the related values of pH at the right-hand-side.

**Table 2**
Formation constants used for the construction of the stability regions given in Fig. 2.

| Species | Formation constant | Value | Reference |
|---|---|---|---|
| $(UO_2)_2(OH)_2^{2+}$ | lg $K_{22}$ | −6.1 | [22] |
| $(UO_2)_3(OH)_5^{+}$ | lg $K_{35}$ | −17.1 | [22] |
| $L^-$ | p$K_{HL}$ | 2.9 | [39] |
| $[UO_2L]^+$ | lg $K_{UL}$ | 2.1 | this study |

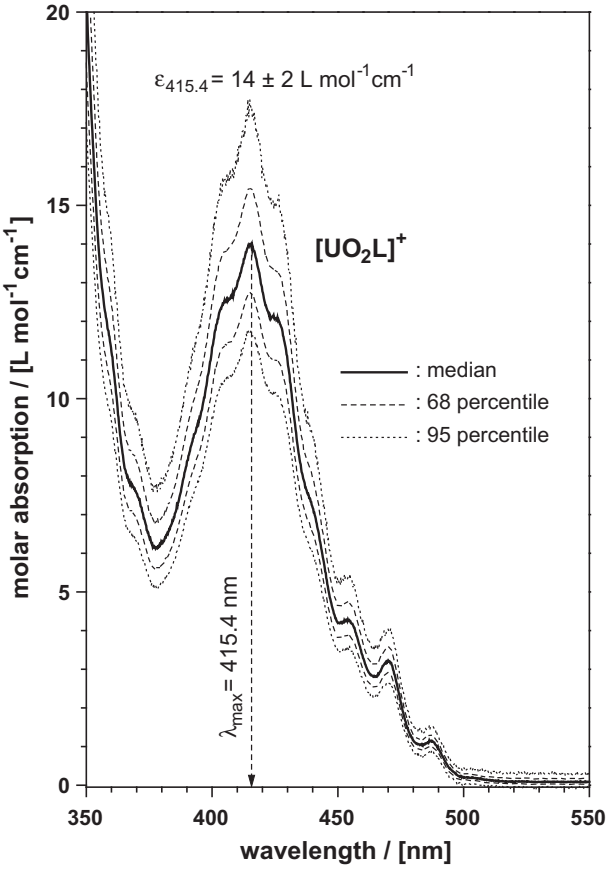


**Fig. 6.** Single component spectrum of species $UO_2L^+$ as obtained from TBCAT analysis of the spectra Fig. 5. Together with the median spectrum, TBCAT also estimates the 68% and 95% confidence limits on basis of the influence factors and their respective magnitudes given in Table 3.

multi-component mixture is known. This known component can be, for example, the UV–Vis absorption spectrum of the uncoordinated metal species. Factor analysis is a widely used chemometric technique. Further details have been given in the literature. The procedure decomposes a matrix A of experimental spectra into two matrices $\mathbf{E}^*$ and $\mathbf{C}^*$. The information on single component spectra of the species and their respective concentrations in matrices $\mathbf{E}^\#$ and $\mathbf{C}^\#$ is given in a mathematical form of eigenvectors that need to be transformed into physically meaningful values. This transformation step is known as target rotation using an $n \times n$ rotation matrix **T**:

$$\mathbf{E}^* = \mathbf{E}^\#\mathbf{T} \quad (2)$$

$$\mathbf{C}^* = \mathbf{C}^\#\mathbf{T}^{-1} \quad (3)$$

where the superscript −1 represents the inverse of matrix **T**. The task of TBCAT is to find a suitable transformation matrix **T** and its optimum dimension $n$ on basis of the constraints inherent in the system: non-negative absorption values in matrix $\mathbf{E}^*$ and non-negative concentration values in matrix $\mathbf{C}^*$. The single component spectra in the columns of matrix $\mathbf{E}^*$ are simultaneously obtained from the same transformation matrix **T** as are the concentration values in matrix $\mathbf{C}^*$. Since the number of species $n$ is a crucial value in the overall analysis resulting in **T**, the search strategy implemented in TBCAT searches for suitable solutions at several values for $n$. In some cases more than one solution compatible with all constraints may be obtained [26].

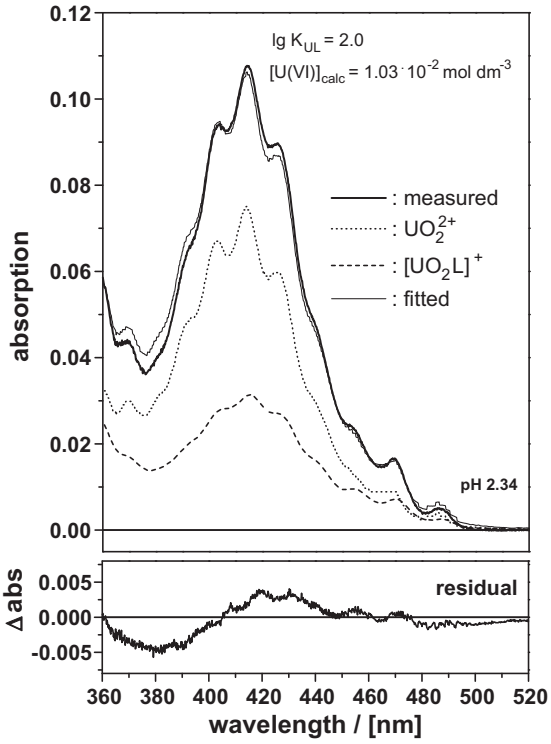


**Fig. 7.** Numerical interpretation (least squares fit) of an experimental spectrum at pH 2.34 by the single components $UO_2^{2+}$ and $UO_2L^+$.

Fig. 6 presents as a result the single component spectrum of the $[UO_2L^+]$ species. The maximum molar absorption is about $(14 \pm 2)$ L mol$^{-1}$ cm$^{-1}$ at 415.4 nm. An application of this single component spectrum to the interpretation of the UV–Vis spectrum collected at pH 2.34 is shown in Fig. 7. The evaluated formation constant is lg $K_{UL}^+ = 2.0$ for this individual spectrum. For the purpose of comparability of experimental results with other studies a measure of the likely range of a result is required. This likely range should encompass all influence factors affecting the result. TBCAT is using computer-intensive resampling algorithms in conjunction with classical Monte Carlo strategies to obtain such an estimate. The influence factors taken into account in the current study are given in Table 3 together with their magnitudes.

The misfit in the calculated sum spectra and the experimentally measured spectra is taken into account by the threshold bootstrap resampling procedure. Threshold bootstrap accounts for correlation, non-normality and non-linearity within the experimental data [26,36,37]. On that basis the complete measurement uncertainty budget has been obtained as a range between the 0.16 percentile and the 0.84 percentile of the empirical distribution function of the evaluated formation constant lg $K_{UL}$ shown in Fig. 8. This relates to lg $K_{UL} = 2.1 \pm 0.1$. The complete measurement uncertainty budget for lg $K_{UL}$ is shown in Fig. 8 by its probability distribution.

The value of the formation constant lg $K_{UL}$ is in the order of magnitude found previously for the $UO_2SO_4$ species [26] and contrasts considerably with the formation constant of the $UO_2CO_3$

**Table 3**
Influence factors and their estimated uncertainty contribution[a].

| Influence factor | Quantity | Uncertainty estimate $u_c$ | |
|---|---|---|---|
| Uranium concentration | $[U]_{total}$ | 3.75% | relative |
| Ligand concentration | [isonicNO] | 4% | relative |
| Acidity constant of isonicNO | $pK_{isonicNO}$ | 0.2 | absolute |
| UV–Vis absorption | $A$ | 2% | relative |

[a] Spectroscopic misfit between the optimum calculated sum spectra and the experimental spectra is taken into account by the threshold bootstrap algorithm.

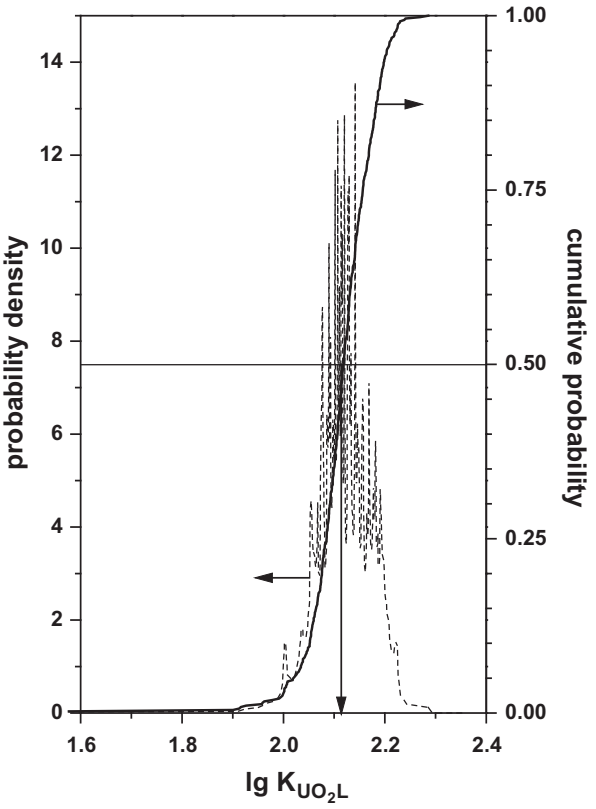


**Fig. 8.** Empirical probability density of the formation constant lg $K_{UL}$ as obtained from multivariate analysis by TBCAT on basis of the influence factors listed in Table 3.

species [30]. Mean values of formation constants of a few single ligand uranyl compounds are given below. Carbonate [30], acetate [28] and nitrate [29] form bidentates with U(VI). Here, the bond angle between chelating oxygen groups in the ligand is always smaller than 60°. Such ligands are referred to as 'short-bite' ligands. Sulfate is not a short-bite ligand. Coordination as a single ligand is the only option for the U(VI) monosulfato species.

$UO_2CO_3^\circ$ : $\lg K = 8.8$ [30]
$UO_2CH_3COO^+$ : $\lg K = 3.8$ [40]
$UO_2L^+$ : $\lg K = 2.1$ this work
$UO_2SO_4^\circ$ : $\lg K = 1.8$ [26]
$UO_2NO_3^-$ : $\lg K = -1$ [40]

The few examples illustrate that there is no simple correlation between the mode of coordination and the strength of the formation constant. Hence the question arose whether the $L^-$ ligand, as a bifunctional species, might coordinate to the uranyl group as a bidentate via the carboxylate group, or as a monodentate via the N–O group.

Due to the complete lack of crystallographic information on isonicotinic acid N oxide compounds with uranyl, experiments were initiated to obtain suitable compounds.

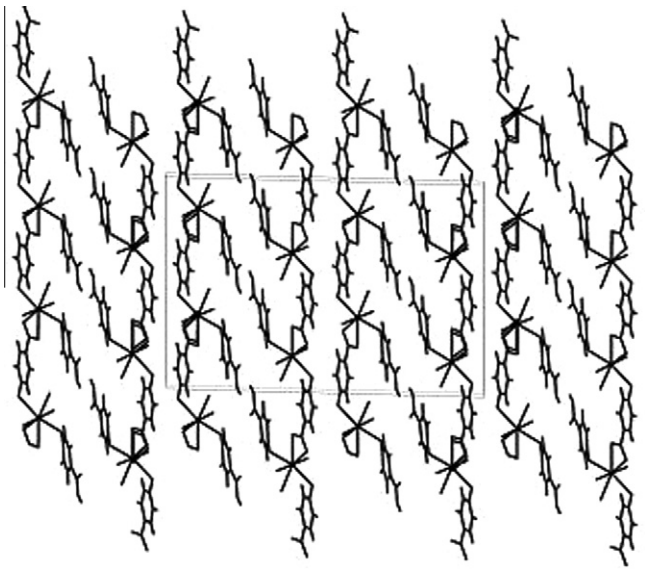

**Fig. 9.** Structure of $[UO_2Cl(HL)L]_n$. seen along the $x$-axis. The unit cell is included.

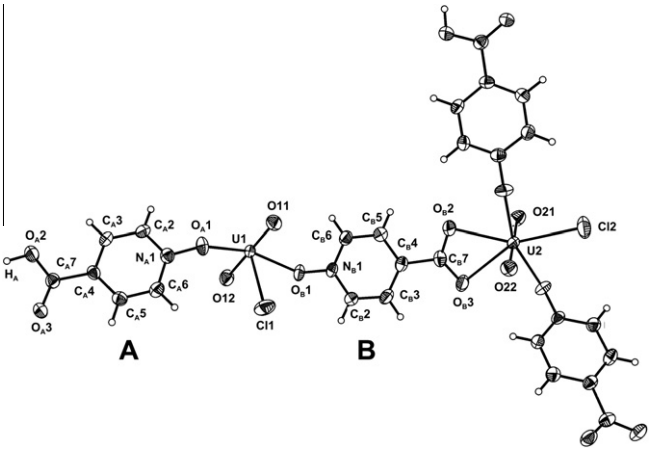


**Fig. 10.** Sheet section of $[UO_2Cl(HL)L]_n$ showing the different links formed by uranyl entity and the ligands HL (group A) and $L^-$ (group B).

### 3.1. Crystallographic study

Due to the complete lack of U(VI) compounds with isonicotinic acid N oxide, single crystals were obtained from a $UCl_4$ solution holding isonicotinic acid N-oxide. Details of the crystallographic analysis of this compound are given elsewhere [41].

The crystal is monoclinic. The stoichiometry U(VI):HL:L:Cl is 1:1:1:1. Thus, each uranyl center is coordinated by a $L^-$ ligand where the carboxylate group acts as a bidentate, by an $L^-$ ligand where the N–O group acts as a monodentate ligand, a HL ligand where the N–O group acts as a monodentate ligand and a $Cl^-$ ligand. An $L^-$ ligand links two uranyl centers acting as a bidentate ligand via its carboxylate group and as a monodentate *via* its N–O group, as shown in Fig. 9. The chains are linked not only via

**Table 4**
Geometry data of $L^-$ and HL molecules obtained from DFT simulations and X-ray crystallography.

| Items | DFT | X-ray | X-ray |
|---|---|---|---|
| | Solution | B ($L^-$) | A (HL) |
| Distance | [pm] | [pm] | [pm] |
| $N_x1$–$O_x1$ | 130.3 | 132.6(3) | 132.7(3) |
| $N_x1$–$C_x2$ | 137.3 | 135.1(4) | 134.9(4) |
| $C_x2$–$C_x3$ | 138.6 | 137.9(4) | 136.6(5) |
| $C_x3$–$C_x4$ | 140.3 | 138.2(5) | 138.5(5) |
| $C_x4$–$C_x5$ | 140.1 | 138.4(4) | 138.4(4) |
| $C_x5$–$C_x6$ | 138.7 | 136.3(5) | 136.5(5) |
| $C_x6$–$N_x1$ | 136.9 | 134.7(4) | 135.6(4) |
| $C_x4$–$C_x7$ | 155.1 | 150.7(5) | 148.3(4) |
| $C_x7$–$O_x2$ | 125.7 | 126.0(4) | |
| $C_x7$–$O_x3$ | 130.2 | 126.2(4) | 122.4(4) |
| $C_x7$–$O_x2$(H) | | | 130.9(4) |
| *Angle (°)* | | | |
| $O_x2$–$C_x7$–$O_x3$ | 131.0 | 121.2(3) | 124.7(3) |
| $O_x2$–$C_x7$–$C_x5$–$C_x6$ | 4.5 | 15.7(5) | 1.9(5) |

Subscript *x* refers to A and B, respectively. The atom numbering for ligand $L^-$ in solution is analogous.

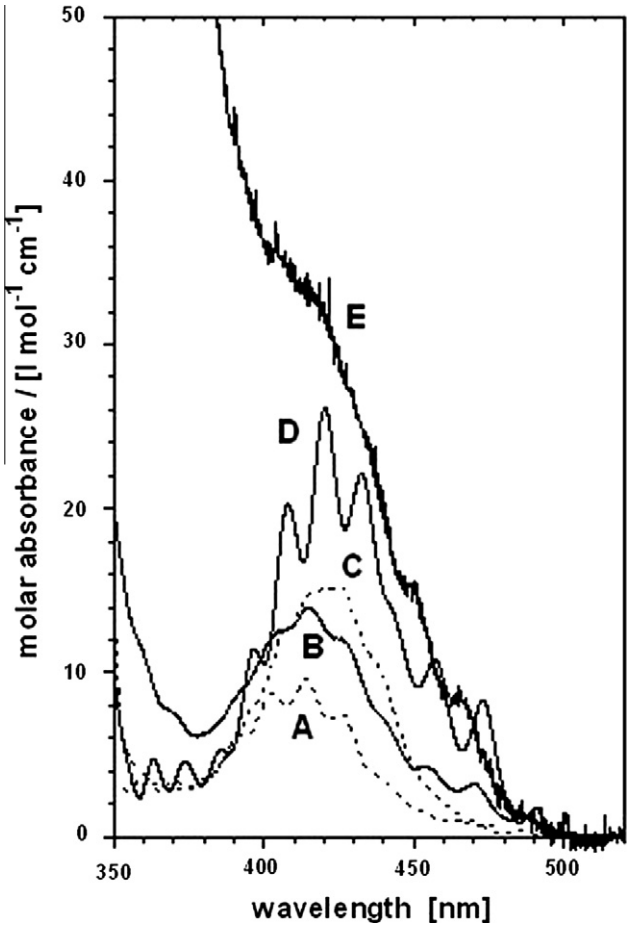


**Fig. 11.** Single component spectra reported for uranyl(VI) with various ligands and 1:1 stoichiometry: A: hydrated uranyl ($[UO_2(OH_2)_5]^{2+}$ as a reference). B: $[UO_2(OH_2)_3CH_3COO]^+$ [27], C: $[UO_2(OH_2)_3NO_3]^+$ [29], D: $[UO_2(OH_2)_4SO_4]$, [26] and E: $[UO_2(OH_2)_3CO_3]$ [30].

the uranyl centers but also *via* HL ligands linking two carboxylic acid groups by hydrogen bonding. Thus HL groups bind with the uranyl centers only *via* the N–O groups while $L^-$ groups link uranyl centers using both functional groups. Chloride atoms saturate the coordination sphere of each uranyl center. The uranyl centers are equatorially pentacoordinated.

Table 4 gives interatomic distances and bond angles from crystallographic analysis in the $L^-$ and HL groups as well as those calculated for $L^-$ from DFT methods. The major difference is observed in the interatomic distance between $C_x4$ and $C_x7$ where the calculated value is almost 7 pm higher than the shortest value obtained from the crystal data (Fig. 10). The otherwise close agreement puts some confidence in the values calculated for the dipole moments (cf. Table 1).

While the crystal structure analysis reports the first data on uranyl(VI) compounds with isonicNO, it does not give an unambiguous hint on the likely interaction of $L^-$ in solution. For the time being, the dependence of U(VI) complexation by isonicNO on pH gives evidence to uranyl coordiantion by the carboxylate group. Assuming uranyl coordination by the N–O group does not result in a satisfactory numerical interpretation by TBCAT analysis.

## 4. Conclusions

This study was motivated by four reasons: the complete lack of qualitative and quantitative information on interaction of pyridine carboxylic acid N-oxides with uranyl. The extension of the currently rather small data, base on single component UV–Vis spectra of 1:1 complexes with uranyl. Görller-Walrand et al. [27–29,42] have suggested coordination geometry as a relevant factor affecting the shape of U(VI) absorption spectra in the solid state and in aqueous solution. Fig. 11 summarizes the single component spectra of U(VI) single ligand species from different sources in the range 350–550 nm. This range encloses the characteristic absorption of uranyl(VI). Toward lower wavelength, almost continuous intense absorption extents without characteristic features suitable for spectroscopic speciation.

The general observation that coordination of the $[UO_2(OH_2)_5]^{2+}$ by ligands other than water increases the maximum molar absorption is also valid for the single ligand species. However, there are no features characteristic for the single ligand species. The almost symmetric band found for the $[UO_2L]^+$ species (cf. Fig. 6) corresponds to $[UO_2(OH_2)_3CH_3COO]^+$ [27], but is clearly different from the monosulfato species. The U(VI) monosulfato species, however, is the only U(VI) single ligand species with known UV–Vis absorption spectrum forming a monodentate interaction between uranyl and ligand. For the other species, bidentate coordination may be assumed. The monosulfate species is also the only of the single ligand species showing a clear band structure in its UV–Vis absorption spectrum. In summary, however, the small database does not allow to draw any conclusion with some reliability. Thus, this work calls for further speciation activity to improve the situation.

The procedures to decompose multi-component spectra into single components are largely undocumented in the literature before the advent of chemometric methods. With multivariate mathematical tools and digital calculators with sufficient memory, multivariate analysis of UV–Vis spectra has become rather popular. If absorptions are measured for a given chemical system at *k* wavelengths, *k* simultaneous linear equations of the type of Eq. (3) are obtained. The concentrations $c_i$ in a sample are the same if the wavelengths are varied, while the molar absorptions $\varepsilon_{i\lambda}$ of each species are the same in all samples if the concentrations are varied. Thus, for a given set of *n* species the spectra obtained at a larger number of *k* wavelengths in *i* samples can be conveniently expressed as a matrix:

$$\mathbf{A} = \mathbf{EC} \tag{4}$$

where the absorptions $a_{ik}$ in matrix **A** have been obtained at the same *d*. The singular value decomposition is an efficient algorithm

to decompose the matrix **A** into two matrices of eigenvectors $\mathbf{E}^{\#}$ and $\mathbf{C}^{\#}$. If the number $n$ of species in solution is known, matrix $\mathbf{E}^{\#}$ with dimensions $i \times k$ can be reduced to dimensions $i \times n$. Similarly, matrix $\mathbf{C}^{\#}$ can be reduced to matrix $\mathbf{C}^{*}$ with dimensions $n \times k$. Hence, the first task is to identify $n$.

The matrices $\mathbf{E}^{*}$ and $\mathbf{C}^{*}$ are still not appropriate estimates of the true but unknown matrices **E** and **C** (cf. Eq. (4)) only hold row and column eigenvectors of matrix **A**. While these eigenvectors are mutually orthogonal to each other, they have no physical meaning but may hold, for instance, negative values. Absorptions and species concentrations, however, have to be non-negative. To obtain physically meaningful estimates of single component spectra and species concentrations, the transformation matrix **T** (cf. Eqs. (2) and (3)) has to be found. Finding an appropriate **T** is crucial for the complete procedure. While matrices $\mathbf{E}^{\#}$ and $\mathbf{C}^{\#}$ are obtained by a well-known numerical algorithm automatically, finding an appropriate **T** poses two problems:

1. The dimension of **T** is $n \times n$. So $n$ must be known.
2. The elements $t_{lm}$ ($l = 1–n$, $m = 1–n$) of **T** can be any real number. There are no symmetry arguments or other constraints (e.g. **T** does not have to be semiidempotent).

There have been a variety of attempts to find mathematical arguments indicating 'optimal' pure variables. As a matter of fact; the presence of uncertainties (named as disturbances, residuals, errors etc.) reduces the validity of most of these approaches. All programs, including TBCAT, have to define a criterion for iterative optimisation. As a weak point in these algorithms the minimisation procedure was identified. Levenberg–Marquardt minimisation or Newton–Raphson procedures are frequently used as iterative algorithms for optimisation. These methods, however, require derivatives to locate the minimum of the optimisation routine and, consequently, a mathematical expression of the relationship between the parameters and the optimisation criterion.

Optimising **T** directly by an iterative algorithm has not yet chosen in order to perform the optimisation according to Eqs. (2) and (3). There exist derivative-free iterative optimisation algorithms, e.g. the Simplex. Thus, computer-assisted target factor analysis (CAT) is the only known code directly optimising the elements of matrix **T** with respect to several constrains simultaneously. A key element in TBCAT's optimisation is the availability of a known component in the multi-component mixture. This component is usually the hydrated ('free') metal ion, where the single component spectrum can be obtained from an acidic solution. The second criterion is the non-negativity of absorptions and species concentrations in matrices $\mathbf{E}^{*}$ and $\mathbf{C}^{*}$. The number $n$ is not inferred from a statistical test or any other auxiliary criterion but tested numerically for a range of values. If the system is underdetermined, a considerable misfit results. If the system is over-determined, the excess parameters will interpret the same information and, as a result, the spectral shapes of these 'excess' single components will include either negative absorption and/or mimic an already existing single component spectrum. The consistency of the numerical solution can be assessed independently because the species concentrations in matrix $\mathbf{C}^{*}$ must sum up to the total metal ion concentration in solution (which is not optimised), while the total amount of ligand must not exceed the added total ligand concentration (a value which is also not optimised). Furthermore, from the solution conditions of each of the $k$ samples and the calculated single species concentrations, formation quotients can be estimated which likewise have to be consistent for all samples. It must be emphasised that the matrices $\mathbf{E}^{*}$ and $\mathbf{C}^{*}$ are obtained from the eigenvectors by same transformation matrix **T**, because $\mathbf{T}^{-1}$ is just the inverse of **T**. Thus, a single component spectrum as suggested for $[UO_2L]^{+}$ (cf. Fig. 6) results from rather narrow constraints. The complete measurement uncertainty budget, which is estimated by a combination of threshold bootstrap (TB) and Monte Carlo simulation, does not only account for numerical misfit but also attempts to include the relevant influence factors. Details on these aspects can be found elsewhere [26,36,37]. The numerical optimisation for a given $n$ runs completely automatic – user input is required in defining $n$, specifying some starting values (where Simplex algorithm is much less sensitive to starting conditions compared to, e.g., the Newton–Raphson method) and setting the stoichiometry of the system. Nevertheless, finding a satisfactory solution may become tedious. Occasionally, two possible solutions for a system may be found where additional reasoning is necessary to decide for the more probable result [26]. Any set of single component spectra should be applied to the resolution of suitable multi-component spectra, which have not been included into the data set for the evaluation of the single component spectra (cf. Figs. 4 and 7).

The results of that study allow some optimism that a spectroscopic study of U(VI) complexation by nicotinic acid N-oxide may provide conclusive results. The acidity constant of nicotinic acid N-oxide is slightly higher compared to that of isonicotinic acid N-oxide while the calculated dipole moment of nicotinic acid is considerably larger. Because U(VI) is considered as a hard Pearson acid, the higher dipole moment of nicNO might result in a higher formation constant compared to isonicNO. For picolinic acid N-oxide, the situation is more complex because U(VI) coordination by picNO may involve both the carboxylate group and the N–O group [43].

## References


[1] A. Albini, S. Pietra, Heterocyclic N-oxide, CRC Press, Boca Raton, USA, 1991.
[2] J. Balzarini, M. Stevens, E. De Clerc, D. Schols, C. Pannecouque, J. Antimicr. Chem. Chem. 16 (1977) 3314.
[3] N.A. Al-Masoudi, Y.A. Al-Soud, I.A. Al-Masoudi, Sulfur Lett. 24 (2000) 13.
[4] B.-X. Li, R.-L. Shang, B.-W. Sun, Acta Cryst. E64 (2008) m131.
[5] S. Lis, Z. Piskula, M. Kubicki, Mater. Chem. Phys. 114 (2009) 134.
[6] G.F. de Sa, O.L. Malta, C. de Mello Donega, A.M. Simas, R.L. Longo, P.A. Santa Cruz, E.F. da Silva Jr., Coord. Chem. Rev. 196 (2000) 165.
[7] S. Lis, Z. Piskula, M. Puchalska, J. Legendziewicz, J. Luminescence 122–123 (2007) 221.
[8] G. Meinrath, S. Lis, U. Böhme, J. Alloys Compd. 408–412 (2006) 962.
[9] M. Borkowski, S. Lis, G.R. Choppin, Radiochim. Acta 74 (1996) 117.
[10] E. Rabinovitch, R.L. Belford, Spectroscopy and Photochemistry of Uranyl Compounds, Pergamon Press, Oxford, UK, 1964.
[11] G. Meinrath, J. Radioanal, Nucl. Chem. 224 (1997) 119.
[12] G. Meinrath, Y. Kato, T. Kimura, Z. Yoshida, Radiochim. Acta 82 (1998) 115.
[13] I.S. Ahuja, R. Singh, R. Sriramulu, Transition Met. Chem. 3 (1978) 193.
[14] N.W. Alcock, W. Errington, T.J. Kemp, J. Leciejewicz, Acta Crystallogr., Sect. C 52 (1996) 615.
[15] E.V. Grechishnikova, E.V. Peresypkina, A.V. Virovets, Yu.N. Mikhailov, L.B. Serezhkina, Russ. J. Coord. Chem. 33 (2007) 458.
[16] R.G. Denning, Struct. Bond. 79 (1992) 215.
[17] Ch.K. Jörgensen, Chem. Phys. Lett. 89 (1982) 455.
[18] E.H.P. Cordfunke, The Chemistry of Uranium, Elsevier, Amsterdam, NL, 1969.
[19] I. Billard, E. Ansoborlo, K. Apperson, S. Arpigny, A.E. Azenha, D. Birch, P. Bros, H. Burrows, G.R. Choppin, L. Couston, V. Dubois, T. Fanghänel, G. Geipel, S. Hubert, T. Kimura, J. Kim, R. Klenze, A. Kronenberg, M. Kumke, G. Lamarque, S. Lis, G. Madic, G. Meinrath, C. Moulin, D. Parker, G. Plancque, F. Sherbaum, E. Simoni, S. Sinkov, C. Viallesoubranne, Appl. Spectrosc. 57 (2003) 1025.
[20] G. Meinrath, S. Hurst, R. Gatzweiler, Fresenius J. Anal. Chem. 368 (2000) 561.
[21] M. Aberg, Acta Chem. Scand. 24 (1970) 2901.
[22] G. Meinrath, Radiochim. Acta 77 (1997) 221.
[23] H.S. Dunsmore, S. Hietanen, L.G. Sillen, Acta Chem. Scand. 17 (1963) 2644.
[24] S. Dai, M.C. Burleigh, J.M. Simonson, R.E. Mesmer, Z.-L. Xue, Radiochim. Acta 81 (1998) 195.
[25] G. Meinrath, J. Radioanal. Nucl. Chem. 232 (1998) 179.
[26] G. Meinrath, S. Lis, Z. Piskuła, Z. Glatty, J. Chem, Thermodynamics 38 (2006) 1274.
[27] C. Görller-Walrand, S. de Jaegere, Spectrochim. Acta 28A (1972) 257.
[28] C. Görller-Walrand, S. de Jaegere, J. Chim. Phys. Fr. 4 (1972) 726.
[29] S. de Houwer, C. Görrler-Walrand, J. Alloys Compd. 323–324 (2001) 683.
[30] G. Meinrath, R. Klenze, J.I. Kim, Radiochim. Acta 74 (1996) 81.
[31] G. Meinrath, P. Schneider, Quality Assurance for Chemistry and Environmental Science, Springer, Heidelberg, FRG, 2007.

[32] A.N. Kost, P.B. Terentiev, L.A. Golovleva, A.A. Stolyarchuk, J. Pharm. Chem. 1 (1967) 235.
[33] S. Lis, Z. Hnatejko, P. Barczynski, M. Elbanowski, J. Alloys Compd. 344 (2002) 70.
[34] M.J. Frisch, G.W. Trucks, H.B. Schlegel, G.E. Scuseria, M.A. Robb, J.R. Cheeseman, V.G. Zakrzewski, J.A. Montgomery Jr., R.E. Stratmann, J.C. Burant, S. Dapprich, J.M. Millam, A.D. Daniels, K.N. Kudin, M.C. Strain, O. Farkas, J. Tomasi, V. Barone, M. Cossi, R. Cammi, B. Mennucci, C. Pomelli, C. Adamo, S. Clifford, J. Ochterski, G.A. Petersson, P.Y. Ayala, Q. Cui, K. Morokuma, D.K. Malick, A.D. Rabuck, K. Raghavachari, J.B. Foresman, J. Cioslowski, J.V. Ortiz, A.G. Baboul, B.B. Stefanov, G. Liu, A. Liashenko, P. Piskorz, I. Komaromi, R. Gomperts, R.L. Martin, D.J. Fox, T. Keith, M.A. Al-Laham, C.Y. Peng, A. Nanayakkara, C. Gonzalez, M. Challacombe, P.M.W. Gill, B. Johnson, W. Chen, M.W. Wong, J.L. Andres, C. Gonzalez, M. Head-Gordon, E.S. Replogle, J.A. Pople, GAUSSIAN 98. Revision A 7. Gaussian Inc., Pittsburgh.
[35] R.N. Sylva, M.R. Davidson, J. Chem. Soc., Dalton Trans. (1979) 465.
[36] Y. Kato, G. Meinrath, T. Kimura, Z. Yoshida, Radiochim. Acta 64 (1994) 107.
[37] G. Meinrath, S. Lis, Z. Stryla, C. Noubactep, J. Alloys Compd. 300–301 (2000) 107.
[38] G. Meinrath, S. Lis, Fresenius J. Anal. Chem. 369 (2001) 124.
[39] G. Meinrath, T. Kimura, Inorg. Chim. Acta 204 (1993) 79.
[40] JESS Joint Expert Speciation System <http://www.murdoch.edu.au/jess>.
[41] S. Lis, Z. Glatty, G. Meinrath, M. Kubicki, J. Chem. Crystallogr. 40 (2010) 646.
[42] C. Görller-Walrand, S. de Jaegere, J. Chim. Phys. 70 (1973) 360.
[43] S. Lis, Z. Glatty, G. Meinrath, M. Kubicki, unpublished data.